Average Radiative Capture Cross Sections for 7- to 170-kev Neutrons*

J. H. GIBBONS, R. L. MACKLIN, P. D. MILLER, AND J. H. NEILER
Oak Ridge National Laboratory, Oak Ridge, Tennessee

(Received August 17, 1960)

Measurements of neutron radiative capture cross sections in the kev region have been made using fast (millimicrosecond) time-of-flight techniques and a large liquid scintillator tank. Two series of measurements have been completed on a number of nuclides. These are determinations of (1) cross sections relative to that of indium at 30 kev and at 65 kev for 49 elements, and (2) cross sections as a function of neutron energy for the following nuclei: Br, Nb, Pd, Ag, Cd, In, Sb, I, Pr, Sm, Gd, Tb, Dy, Ho, Er, Tm, Yb, Lu, Ta, W, Pt, and Au. Curve fits, using the statistical model, have been obtained for Br, Nb, Ag, In, Sb, I, Pr, Tb, Ho, Tm, Lu, Ta, and Au. The results demonstrate the presence of the $2p$ giant resonance near $A=100$ predicted by the optical model. The average nuclear parameters obtained are in good agreement with recent low-energy total cross-section results, but are in poor agreement with earlier results. Possible reasons for these disagreements are discussed.

I. INTRODUCTION

THE study of neutron capture cross sections has had three principal motivations: nuclear reaction theory, stellar nucleosynthesis theory, and nuclear reactor design. Detailed studies of thermal cross sections (0.025 ev) where capture is the predominant interaction, have been of invaluable aid in reactor design, but of limited help for reaction theory or nucleosynthesis calculations. The energy range downward from about 100 kev and including the ev range is an interesting region from all three points of view. This energy region is characterized by interaction of predominantly s- and p-wave neutrons with generally *only* elastic scattering and radiative capture occurring. Further, theories of nucleosynthesis[1] predict correlations between elemental abundances and neutron capture cross sections in the range 10 to 100 kev. Finally, recent reactor design criteria have been increasingly sensitive to ev- and kev-range capture cross sections.

Some work in the kev range has been performed by activation[2–19] and spherical shell transmission[20,21] techniques. The activation technique is limited to isotopes that activate with convenient half-lives but has the advantages of easy isotope identification and high sensitivity. Spherical shell transmission studies to date have been mostly limited to specific neutron energies available from photoneutron sources, and require very large samples. On the other hand, these measurements provide probably the most accurate absolute absorption cross sections. An almost generally applicable technique for measurement of capture cross sections is the detection of a capture event by observation of the prompt γ radiation. This technique has been applied with a CaF_2 scintillator in a small-solid-angle geometry,[22] and has been most successfully applied to a large liquid scintillator tank in nearly 4π geometry[23] for neutron energies greater than 175 kev where monoenergetic neutrons are readily produced. For neutron energies less than 120 kev, measurements of radiative capture as a continuous function of neutron energy require a more elaborate system. The development of millimicrosecond pulsed beam techniques and fast pre-acceleration pulsing of the ORNL 3-Mv Van de Graaff have enabled us to investigate radiative capture cross sections for a large number of elements from about 7 kev upward to about 170 kev.

* Several preliminary reports of this work have been given: Bull. Am. Phys. Soc. Ser. 4, 43 (1959); Bull. Am. Phys. Soc. 4, 231 (1959); Bull. Am. Phys. Soc. 4, 414 (1959); Bull. Am. Phys. Soc. 4, 474 (1959).

[1] E. M. Burbidge, G. R. Burbidge, W. A. Fowler, and F. Hoyle, Revs. Modern Phys. **29**, 547 (1957).
[2] V. Hummel and B. Hamermesh, Phys. Rev. **82**, 67 (1951).
[3] C. Kimball and B. Hamermesh, Phys. Rev. **89**, 1306 (1953).
[4] R. L. Macklin, N. H. Lazar, and W. S. Lyon, Phys. Rev. **107**, 504 (1957).
[5] R. Booth, W. P. Ball, and M. H. MacGregor, Phys. Rev. **112**, 226 (1958).
[6] A. I. Leipunsky *et al.*, *Proceedings of the Second United Nations International Conference on the Peaceful Uses of Atomic Energy, Geneva, 1958* (United Nations, Geneva, 1958), Vol. 15, p.50 [2219].
[7] M. V. Pasechnik *et al.*, *Proceedings of the Second United Nations International Conference on the Peaceful Uses of Atomic Energy, Geneva, 1958* (United Nations, Geneva, 1958), Vol. 15, p.18 [2030].
[8] S. J. Bame and R. L. Cubitt, Phys. Rev. **113**, 256 (1959).
[9] F. Gabbard, R. H. Davis, and T. W. Bonner, Phys. Rev. **114**, 201 (1959).
[10] W. S. Lyon and R. L. Macklin, Phys. Rev. **114**, 1619 (1959).
[11] A. E. Johnsrud, M. G. Silbert, and H. H. Barschall, Phys. Rev. **116**, 927 (1959).
[12] J. A. Miskel, K. V. Marsh, M. Lindner, and R. J. Nagle, Bull. Am. Phys. Soc. **4**, 475 (1959).
[13] A. T. G. Ferguson and E. B. Paul, J. Nuclear Energy **A10**, 19 (1959).
[14] J. F. Vervier, Nuclear Phys. **9**, 569 (1959).
[15] E. G. Bilpuch, L. W. Weston, and H. W. Newson, Ann. Phys. **10**, 455 (1960).
[16] L. W. Weston, K. K. Seth, E. G. Bilpuch, and H. W. Newson, Ann. Phys. **10**, 477 (1960).
[17] J. L. Perkin, L. P. O'Conner, and R. F. Coleman, Proc. Phys. Soc. (London) **A72**, 505 (1958).
[18] V. N. Kononov, I. I. Staviskii, and V. A. Tolstikov, J. Nuclear Energy **A11**, 46 (1959).
[19] R. C. Hanna and B. Rose, J. Nuclear Energy **8**, 197 (1959).
[20] H. W. Schmitt and C. W. Cook, Nuclear Phys. **20**, 202 (1960).
[21] T. S. Belanova, J. Exptl. Theoret. Phys. (U.S.S.R.) **34**, 574 (1958) [translation: Soviet Phys.—JETP **34(7)**, 397 (1958)].
[22] I. I. Staviskii and I. V. Shapar, 1959 (private communication).
[23] B. C. Diven, J. Terrell, and A. Hemmendinger, Phys. Rev. **120**, 556 (1960).

The results reported in this paper are conveniently divided into two nearly independent experiments. The first was the determination at two or three energies of cross sections relative to that of the standard. For this experiment kinematically collimated neutrons around 0° from the $Li^7(p,n)$ and $T(p,n)$ reactions at energies very close to their thresholds were used, giving 30 kev and 65 kev neutrons, respectively, as discussed in Appendix I. The pulsed beam system for these measurements simply served to reduce background. A similar measurement was made for 167-kev neutrons by using a thin Li^7 target in a lithium-loaded paraffin collimator, essentially the same technique first described by Diven.[23] These sets of measurements resulted in relative cross sections for these three energies.

The second experiment was the measurement of the *shape* of capture cross sections as a function of neutron energy. In this case neutrons were simultaneously produced over a *band* of energies. Energy selection and measurement was done by fast time-of-flight, similar to the technique used for total cross section measurements.[24] The neutrons were produced by using the $Li^7(p,n)$ and $T(p,n)$ reactions with thick targets and the proton energy adjusted to cover the neutron energy ranges 7–70 kev and 20–170 kev, respectively.

II. APPARATUS AND TECHNIQUES

A. Detector and Electronics

The liquid scintillator consists of double-distilled xylene containing 4–5 g/liter *p*-terphenyl and 0.02 g/liter 2, 5-di-(biphenyl)-oxazole. It is contained in a 1.2-meter equilateral cylinder truncated at both ends (45°) to more closely approximate a sphere[25] (see Fig. 1). The inner surfaces are coated with α-Al_2O_3 (Linde A abrasive) in a binder of sodium silicate. Eight five-inch diameter Dumont 6364 photomultiplier tubes view the interior. The phototube frontplates are in direct contact with the liquid; neopreme O-ring seals are held by chamfered compression plates to the 5-inch diameter cylindrical surfaces of the tubes.

The phototubes are connected by cables (RG62/U) of equal lengths in groups of four which are in turn connected by equal lengths to the preamplifier of an ORNL A-8 Linear Amplifier.[26] This is a double-delay-line amplifier[27] producing a positive pulse immediately followed by an almost identical negative pulse. Such a signal has several advantages; the equality of pulse areas minimizes base line fluctuations with high and variable counting rates and the point of axis-crossing between the positive and negative signals provides a reference time which is insensitive to pulse amplitude for a wide range of signal amplitudes. The precision of the reference time is determined by: the linearity of pulse shape over the range of useful signals, the stability of the amplifier base line, the noise figure of the amplifier, and the uncertainty in timing connected with the statistics of the half amplitude point of each signal. The time of axis crossing is determined by proper adjustment of the hysteresis in a circuit especially designed for operation as a "crossover pickoff."[28]

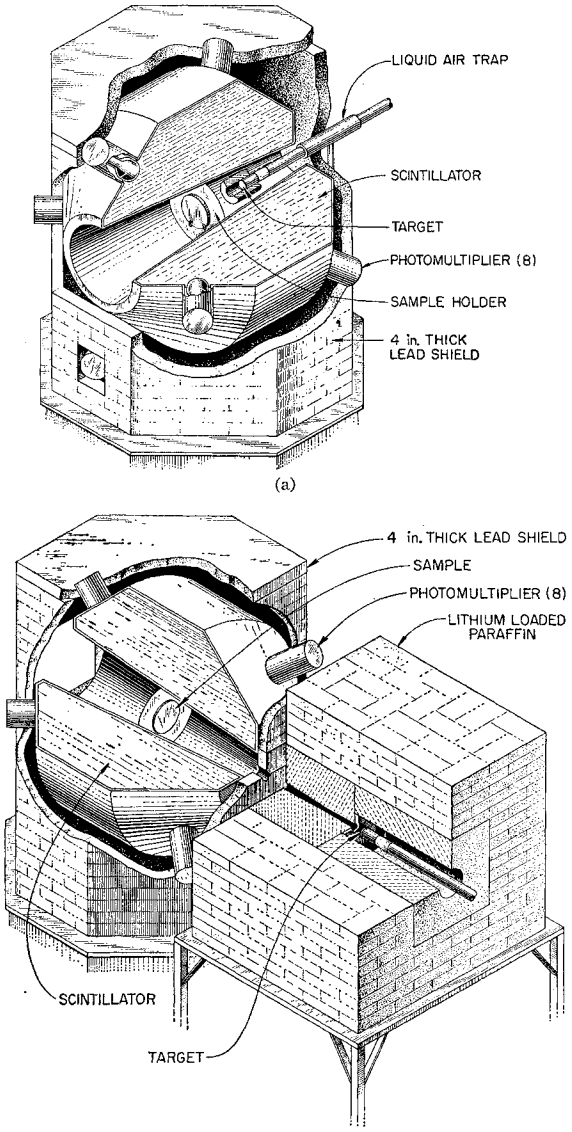

FIG. 1. Liquid scintillator tank as used for measuring (a) capture cross sections with kinematically collimated neutron sources, and (b) capture cross sections as a function of energy.

[24] W. M. Good, J. H. Neiler, and J. H. Gibbons, Phys. Rev. **109**, 926 (1958).

[25] We are indebted to N. H. Lazar for much of the original design work.

[26] G. G. Kelley, Inst. Radio Engrs. Natl. Conv. Record **5**, 63 (1957), Part 2.

[27] E. Fairstein, Rev. Sci. Instr. **27**, 475 (1956).

[28] E. Fairstein, Oak Ridge National Laboratory Instrumentation and Controls Division, Annual Progress Report for Period Ending July 1, 1957 (unpublished). More detailed description may be found in R. W. Peelle and T. A. Love, Applied Nuclear Physics Progress Report, September 1, 1957; Oak Ridge National Laboratory Report ORNL—2389 (unpublished), pp. 245–259.

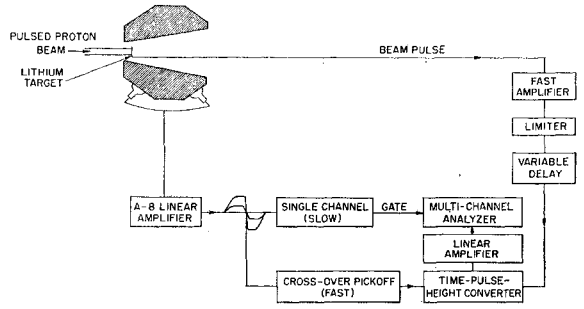

FIG. 2. Block diagram of scintillator tank and associated electronic apparatus, connected for gated time spectrum measurements.

The output of the crossover pickoff provides the prompt or detector input to a time to pulse-height converter which gives an output pulse of amplitude proportional to the time interval between the prompt pulse and the delayed signal produced by the collection of beam pulse on a low capacitance target. A more detailed description of the beam pulsing system and time to pulse-height converter has been published elsewhere.[29] A block diagram of the electronic equipment is shown in Fig. 2. Although test pulser alignment of the crossover pickoff indicated a maximum time jitter of $6-8\times10^{-9}$ sec over the linear-amplifier output-pulse-amplitude range of 7–35 volts, the timing resolution under operating conditions has been $15-25\times10^{-9}$ sec. Base line fluctuations due to high counting rates and large cosmic-ray overload signals probably account for much of the difference. The (p,γ) peak in Fig. 3 shows the time resolution clearly.

The scintillator background pulse-height spectrum is shown in Fig. 4, both with and without the 4-in. Pb shielding. Gamma-ray energies are calibrated in terms of the centroid of the total absorption peak; of course, for Mev energies only a small fraction of γ rays are totally absorbed by the scintillator. A large fraction are not totally absorbed and thus produce smaller pulses. The total efficiency of the scintillator tank for single γ rays from a central source is shown in Fig. 5. This curve was calculated by a Monte Carlo method.[30] The efficiency approaches 97% for very low energies. The difference from unity, 3%, represents the solid angle for escape through the ends of the central duct. Single γ rays of energy equal to high neutron binding

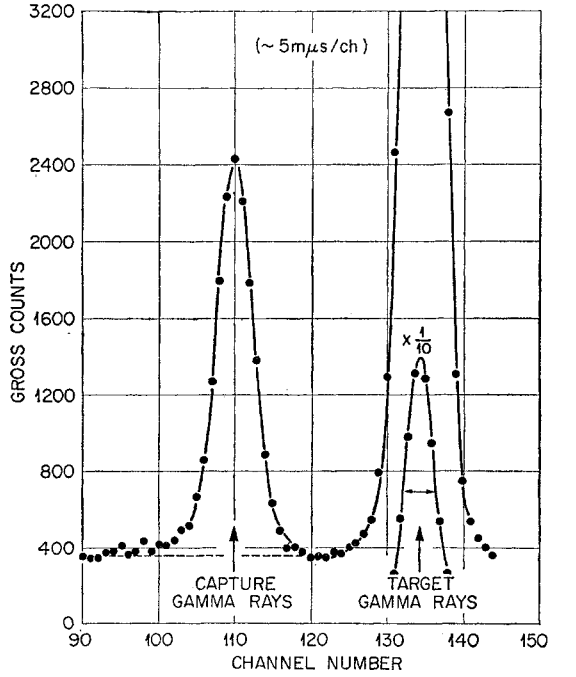

FIG. 3. Flight-time spectrum for 65-kev neutrons incident on a Gd_2O_3 sample. An over-all time resolution of 20×10^{-9} second is indicated by the target gamma-ray peak.

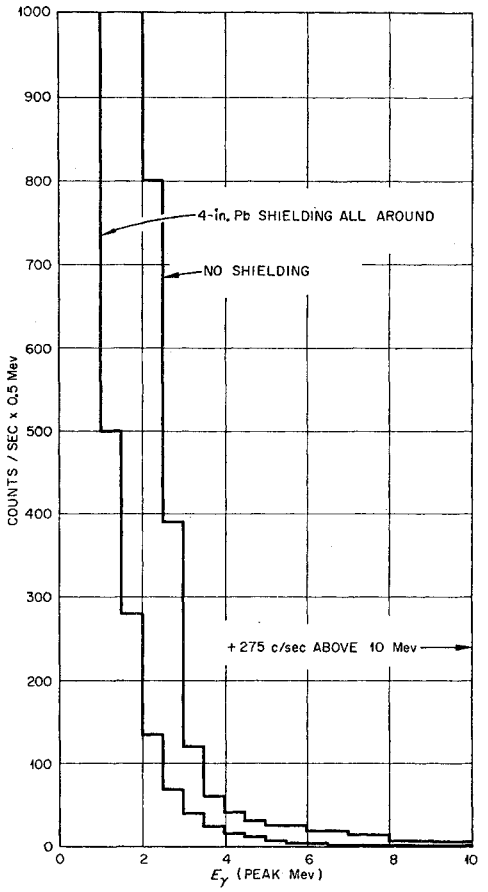

FIG. 4. Background counting rates in scintillator tank with and without 4 in. of lead shielding on all sides, top and bottom.

[29] J. H. Neiler and W. M. Good, *Fast Neutron Physics*, edited by J. L. Fowler and J. B. Marion (Interscience Publishers, Inc., New York, 1960), Chap. IVA.

[30] C. D. Zerby and H. Moran, Oak Ridge National Laboratory —CF–60–5–72 Memo, 1959 (unpublished).

energies have better than a 50% chance to make a light pulse. Since the average multiplicity of decay cascades ranges from 3 to 7,[31] the tank efficiency, for detecting capture, averages well above 90%, with few exceptions.

A principal source of background in earlier measurements was the capture of thermalized neutrons in the scintillator and its container. For this reason, the scintillator was "poisoned" with about 5 liters of trimethyl borate prepared from 97% B^{10}. This addition essentially erased the γ-ray peak at 2.2 Mev (see Fig. 6), due to neutron capture in hydrogen and substituted in its place the much less troublesome peak at 478 kev from the $B^{10}(n,\alpha_1\gamma)Li^7$ reaction. Neutron capture in the central duct wall was minimized by using thin (0.020 in.) Mg as the structural material.

The use of a fast-pulsed (much less than one event per pulse) beam and a fast timing system offers its biggest single advantage in permitting direct measurement of neutron energies by time-of-flight. The same system may, of course, be used in experiments with

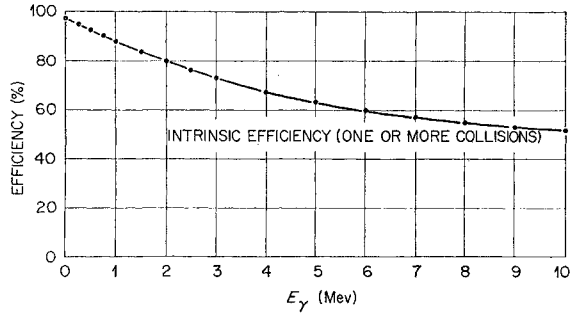

FIG. 5. Intrinsic efficiency of scintillator tank for single gamma rays for producing at least one light pulse. The value (97%) for zero gamma-ray energy represents the solid angle for escape through the collimator hole.

monoenergetic neutrons for reduction of background, as has been pointed out by Diven.[23] Both features were utilized in the experiments described here. The first feature was used in measurements of cross section as a function of neutron energy; the second in measurements of cross section for "monoenergetic" neutrons. A third feature of fast pulsing is that it enables one to study (with no additional sample) capture γ-ray pulse spectra. The time scale of events in the capture tank following a neutron burst is such that, for the fast-pulsed system, one may record background essentially simultaneously with the data, as shown in Fig. 7. To do this is imperative, since the measurement of capture γ-ray pulse-height spectra for low γ-ray energies involves large backgrounds (even with beam pulsing). It is important to determine the background not only with precisely the same amount of neutron scattering but also at essentially the same time as the sample is measured. This selection is made by single-channel analyzers

[31] J. E. Draper and T. E. Springer, Nuclear Phys. **16**, 27 (1960).

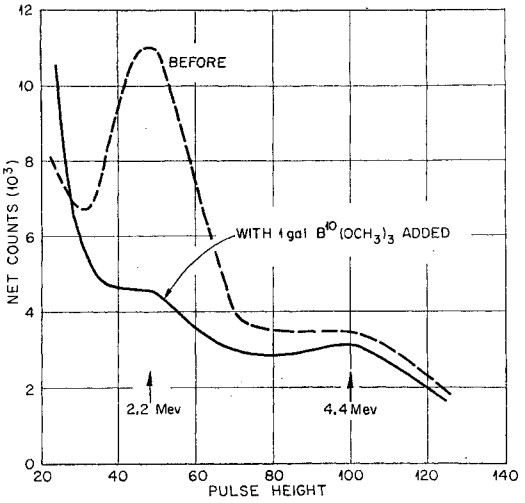

FIG. 6. Pulse-height spectrum in the scintillator tank from a Po-Be neutron and γ-ray source shown with and without B^{10} poisoning.

(Fig. 7) set at two regions in time, one corresponding to the time of neutron capture and the other to a time immediately afterwards (or before) corresponding to only background. The gate signals from each of these single-channel analyzers control concurrent storage in separate halves of the 256-channel analyzer, allowing simultaneous determination of signal and background. The exact ratio of the widths ($\pm 0.5\%$) of the single-channel analyzers is monitored by frequent replacement of the capturing sample with a purely scattering sample (carbon) which provides the same counting rate in the time converter and single-channel analyzers. Whenever capture samples were of such a nature that the *average* counting rates were affected (e.g., with samples with large capture cross sections) the single-channel analyzer window widths were checked at both background and signal counting rates.

B. Samples

The natural element samples used to date have been 5- to 7-inch diameter disks. Metals were used where

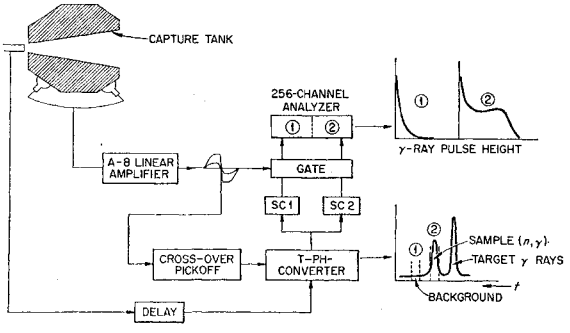

FIG. 7. Block diagram of scintillator tank and associated electronic apparatus connected for capture gamma-ray spectrum measurements.

possible. Pressed oxides and lead salts in thin (0.001 in.) evacuated iron cans were used when necessary. The sample thickness was chosen to give $1/e$ attenuation for about 150-kev gamma rays, and to limit the neutron scattering to a few percent. Samples five times thinner than normal have also been used. Considerably smaller samples (both in diameter and thickness) could be used, but at a proportional sacrifice in a signal to background ratio.

C. Neutron Sources and Shielding

The ORNL 3-Mv Van de Graaff accelerator was pre-acceleration pulsed at 1.6-μsec intervals with pulse durations of about 10 mμsec and *average* proton currents of 1–3 μa. Both lithium and tritium targets were used. The lithium targets were vacuum evaporated metal on Pt and transferred from evaporator to accelerator in a helium atmosphere. The tritium targets were all of the Zr-T type.

For work near the reaction threshold, where neutrons are kinematically collimated into the forward angles, the targets were actually placed *inside* the duct in the scintillator tank as shown in Fig. 1(a). The only shielding used in this case was 1 in. of lead, close around the target, to minimize target γ rays, particularly the 478-kev γ rays from $Li^7(p,p'\gamma)$.

Studies using a broad band of neutron energies (σ vs E measurements) necessitated the use of a lithium-loaded paraffin collimator [Fig. 1(b)]. For effective neutron collimation a shield thickness of about 50 cm was required. A flight path of about 120 cm from neutron source to sample was used.

D. Energy Resolution

The neutron energy spreads encountered in the "monoenergetic" measurements depend *only* upon accelerator control proton beam energy spread, and the chosen accelerator voltage. For the results reported here, the "energy spectra" of neutrons from $Li^7(p,n)$ and $T(p,n)$ were roughly triangular with width at half-maximum of about 15 and 40 kev, respectively. In order to obtain this resolution and a reasonably steady neutron yield, the accelerator, for the case of $Li^7(p,n)$, had to be controlled at 1.883 Mev to better than ± 300 ev. The energy resolution for the measurements at 167 kev was, for all practical purposes, determined only by the lithium target thickness (≈ 3 kev).

The energy resolution in the thick-target experiments (σ vs E) was *independent* of target thickness, accelerator voltage, etc. It depended *only* upon the time resolution and flight path and varied between 44% near 10 kev and 18% near 150 kev.

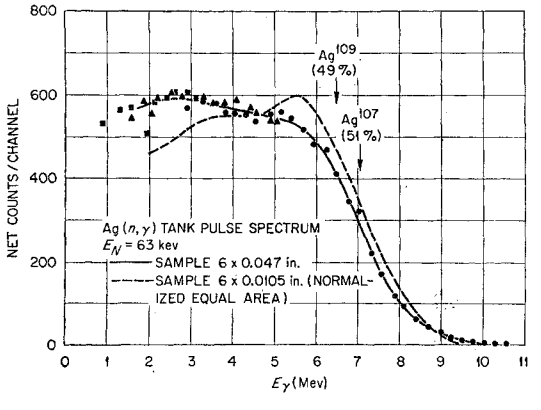

FIG. 8. Net pulse amplitude spectrum of capture gamma rays from two silver samples of different thickness.

III. EXPERIMENTAL RESULTS

A. Measurements Made with Neutrons of 30-, 65-, and 167-kev Energy

The accuracy with which the capture tank can be used to measure cross sections relative to a standard is excellent ($\sim\pm 5\%$) but absolute measurements are much less certain (10–15%). This is due to such uncertainties as (1) neutron flux measurements, (2) total escape probability of capture γ rays, and (3) absolute γ-ray counting efficiency (within the pulse-height window). For this reason, a single standard cross section (measured by a more accurate technique) was chosen and the scintillator tank was used to measure all other cross sections relative to the standard. The "absolute" cross sections thus obtained were then used to normalize results of relative cross section versus energy measurements (to be described in Sec. B).

Use was made of "kinematic collimation" of the neutrons from $Li^7(p,n)$ and $T(p,n)$ very near the reaction threshold to provide intense forward-directed beams of 30- and 65-kev neutrons. The proton energy was adjusted in each case to cause the entire reaction yield to appear within a forward cone of about *10°* half-angle. For the case of $Li^7(p,n)$ for example, at a proton energy 2.0 kev above threshold the number of neutrons ($\bar{E}=30$ kev) incident per second on the sample *during the pulse* is approximately 3×10^8. The experimental arrangement is shown schematically in Fig. 2. Target and sample were separated only enough to clearly differentiate neutrons from target γ rays. In practice the experimental procedure consisted of (1) careful energy calibrations and circuitry adjustment to insure stability of the γ-ray detector bias at a desired pulse height and (2) critical adjustment of the Van de Graaff energy, both in absolute value and stability. Then time spectra were obtained for the various samples, with an indium (standard) sample being run approximately every fourth time, or about once every 15 minutes. The counting rate as a function of time for a typical sample is shown in Fig. 3. The base line (background) increase, due to thermalized neutron captures in the liquid, is a much more probable event

than prompt neutron capture in the scintillator. Since the time required for neutron thermalization and capture is spread out over many pulse cycles, this background is essentially constant and the correction easily made. Fast capture of scattered neutrons was searched for by using a thick carbon sample and found to be completely negligible. The radiative capture cross section for element X is related to the net area under its time peak A_x and to a corresponding area for the standard element A_{std} by

$$\sigma_x=\sigma_{\text{std}}\left(\frac{A_x}{A_{\text{std}}}\right)\left(\frac{\nu_{\text{std}}}{\nu_x}\right)\left(\frac{f_{\text{std}}}{f_x}\right)$$

$$\times(\text{R.S.P. correction})(\text{A.P.L. correction}), \quad (1)$$

where ν=atoms/cm^2, f=fraction of capture γ-ray pulses occurring within the detector single-channel analyzer window, (R.S.P.)=resonance self-protection correction, and (A.P.L.)=scattering correction for average neutron path length in the sample. It is seen that in order to obtain a cross section one must have obtained, in addition to sample-in and sample-out time spectra, the capture γ-ray pulse amplitude spectrum as seen by the scintillator and have determined the corrections for scattering and resonance self-protection (see Appendixes II and III). The spectrum fractions (fraction of the total capture γ-ray spectrum within the γ-ray single-channel window) were obtained by time-gating the multichannel analyzer on, as described in Sec. A, at a time corresponding to the neutron arrival at the sample position, and analyzing capture γ-ray pulse heights. Samples used for capture γ-ray pulse-amplitude spectra measurements were identical to those used in the cross-section measurement. This was important because attenuation of low-energy γ rays, a function of sample thickness, can change the shape of the spectrum (see, for example, Fig. 8).

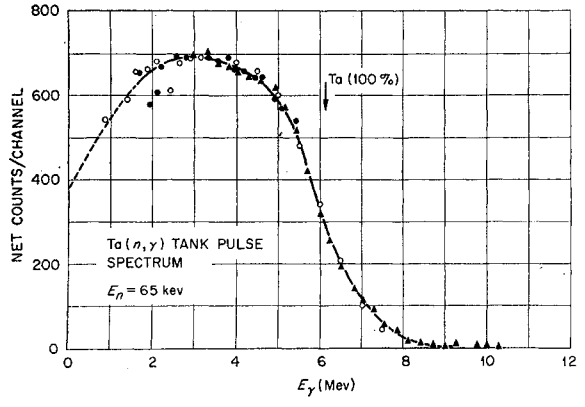

FIG. 9. Net pulse amplitude spectrum of gamma rays from tantalum. The midpoint of the break in the curve at higher energies corresponds, as expected, to the neutron binding energy. The dashed line at lowest energies is the extrapolated shape to zero pulse height. The various symbols represent different experimental runs.

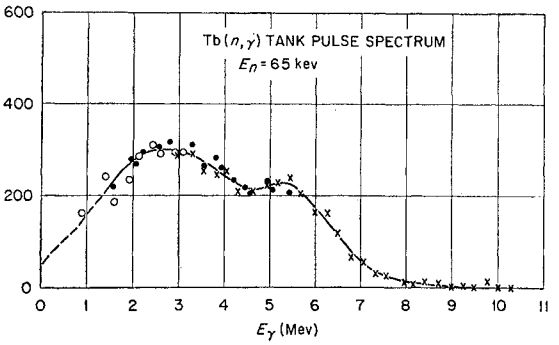

FIG. 10. Net pulse amplitude spectrum of capture gamma rays from terbium. There appears to be definite evidence near 4.5 Mev of some gross structure even under conditions of gamma ray summing in the capture tank. This may be due to preferential dipole transitions to a bound single-particle state. Different symbols represent different experimental runs.

The capture γ-ray pulse-amplitude distributions were taken during a separate run. Typical results are shown in Figs. 9 and 10. Energy calibration for the tank was done with 2.2-Mev γ rays from neutron capture in hydrogen and from the two gamma rays (and their sum peak) from the decay of Na^{24}. As expected, few capture events are observed at the full energy peak, but the midpoint of the break in γ-ray yield corresponds closely to the neutron binding energy as indicated in the figures. The spectra generally fall off gradually at lower γ-ray energies, indicating that few capture events occur that give only a single small pulse in the tank. Some gross structure may be present (see, for example, Fig. 10). This may be due to preferential dipole γ decay via bound single particle states. Such events have also been observed in capture of thermal neutrons.[32]

It is interesting to note the dependence of the fraction of total pulses above a given energy bias upon neutron binding energy. This dependence (Fig. 11) was examined after experimental spectrum fractions had been determined and adds to our confidence in the spectrum fractions. It also gives one an estimate of the spectrum fraction for other elements whose neutron binding energies are known. This is important for samples with cross sections too small ($\lesssim$50 mb) for spectrum measurement.

Absolute Normalization of Cross Sections

The most direct, and most accurate measurements of absolute neutron absorption cross sections in the kilovolt region, have been made by Schmitt and Cook[20] using 24.0-kev neutrons with the spherical shell transmission technique. The best five of these measurements, listed in Table I with their standard deviations, were used to provide normalization for the present experiment in the following manner:

The capture tank measurements of the shapes of the

[32] L. V. Groshev *et al.*, *Atlas of γ-ray Spectra from Radiative Capture of Thermal Neutrons* (Pergamon Press, New York, 1959).

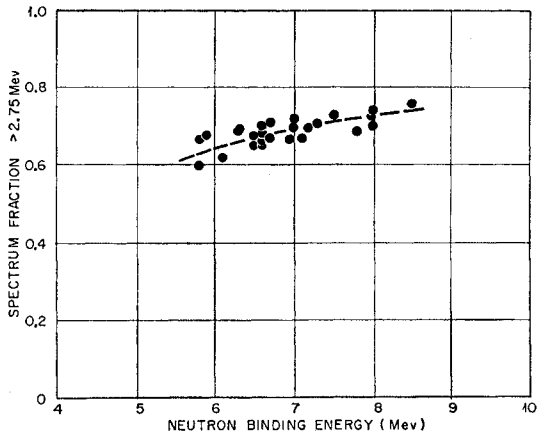

FIG. 11. Fraction of capture gamma-ray pulses observed above 2.76 Mev as a function of neutron binding energy. The apparent regularity as evidenced by these data allow estimates of "spectrum fractions" for nuclei whose cross sections are too small to allow capture gamma-ray measurements. The small scatter of the points demonstrates the relative insensitivity of the scintillator to different types of gamma-ray cascades.

five cross sections as a function of neutron energy were used to extend the spherical shell cross sections to 30 kev. The five elements were then compared at 30 kev by the threshold method described in this paper. The five ratios $\sigma_{\text{shell}}/\text{“}\sigma_{\text{tank}}\text{”}$ were then formed, and the average ratios weighted by the standard deviation of the corresponding σ_{shell} formed. The absolute errors of the five spherical shell determined cross sections range from 6.8 to 10.3%. We assign an absolute error of 6% associated with this normalization. The weighted indium cross section resulting from this normalization at 30 kev is 760±50 mb. The capture cross section of indium at 65 kev was obtained by measuring the ratio of the 65 to 30 kev cross sections. This ratio was found by two different methods. The *relative* neutron fluxes for the Li(p,n) (30 kev) neutrons and the T(p,n) (65 kev) neutrons were measured using the B^{10}—NaI detector described by Good, Neiler, and Gibbons.[24] Assuming the $B^{10}(n,\alpha_1\gamma)Li^7$ cross section to be proportional to $1/v$ in this range,[15,33,34] the ratio of the indium cross section at 65 kev to that at 30 kev is found to be 0.597. The second method of comparing the 65- to 30-kev capture cross sections of indium utilized activation of an indium foil first in the flux of 65-kev neutrons and then in the flux of 30-kev neutrons, the flux of neutrons being measured by the 4π graphite sphere[35] detector. The cross-section ratio determined by this method was 0.583. The average of these two numbers was used to give $\sigma_{\text{In}}=450\pm40$ mb at 65 kev.

The indium capture cross section at 167 kev was determined by normalizing the relative indium cross section versus neutron energy curve at 30 and 65 kev and reading the value as measured by the shape of the U^{235} absorption cross section. The indium cross section shape measurement will be described in Sec. B. The source of 167-kev neutrons was a thin (~3 kev) lithium target placed in a collimator-shield outside the tank, as described later in this article. The number thus obtained was $\sigma_{\text{In}}(167\text{ kev})=258\pm40$ mb.

A summary of the results for all measurements to date is given in Table II. Note that the limit of sensitivity is less than a millibarn. The results at 65 kev for even Z and odd Z were plotted separately on semilog paper and then overlapped and normalized. The

TABLE I. Results of selected shell transmission measurements and comparison with capture tank results. These are the five results chosen to form the average, weighted standard discussed in the text. The first column gives the results of Schmitt and Cook.[a] Results of threshold measurements are given in column 2, and the ratio of results at 24 kev are in column 3. The total spread in the five results is 14%.

Element	σ_{24}(shell)	σ_{30}(tank)	σ_{24}(shell)/σ_{24}(tank)
Ag	1185±80	951	1.05
Sb	565±45	436	1.03
In	823±60	763	0.91
Au	585±60	515	0.93
I	885±90	733	1.04

[a] See reference 20.

TABLE II. Results of "threshold" measurements with 30, 65, and 167 kev average energy neutrons. Capture cross sections are given in millibarns. The estimated absolute error (standard deviation) as discussed in the text is ±10% except where noted. The neutron energy resolution was approximately triangular with width at half-maximum of ±7 and ±20 kev at 30 and 65 kev, respectively, and about ±3 kev at 167 kev.

Element	30	65	167	Element	30	65	167
C	0.2±0.4	0.0±0.3	1.3±2	Pr	115	59	
F	4.5±1.0			Sm	875	450	330
Mg	0.4±0.2	2.1±0.7		Gd	1175	670	310
Al	2.8±0.7			Tb	1850	1070	600
Si	13±4			Dy	775		240
S	25±8						
V	30±8			Ho	1720	1070	515
Cr	10±3	3.5±1		Er	960		230
Fe	12±3	6.3±2		Tm	1310	700	400
Co	88±30			Yb	575	390	170
Ni	16±4	6.5±2		Lu	2520	1200	
Cu	39±7	25±5		Ta	735	440	270
Zn	31±6	20±5		W	270	190	
Ge		39±6		Pt	330	234	
Br	650	345		Au	515	332	230
Sr	155	24		Hg	295	103	
Y	13.5±3	6.9±2		Tl	71	35	
Zr	14±3	10.3±2		Pb	3±3	1±2	
Nb	264	135		Bi	1±4	4±3	
Mo	140	69		U(238)	473	302	
Rh		540					
Pd	454	265	175				
Ag	951	586	375				
Cd	330	183					
In	(763)	(448)	(258)				
Sn	88±15	51±10					
Sb	436	245					
I	733	440					
La	55±10	18±3					
Ce	35±5	8.0±2					

[33] J. H. Gibbons and R. L. Macklin, Phys. Rev. **114**, 571 (1959).
[34] H. Bichsel and T. W. Bonner, Phys. Rev. **108**, 1025 (1957).
[35] R. L. Macklin, Nuclear Instr. **1**, 335 (1957).

resulting curve obtained ($\bar{\sigma}$ vs A) is given in Fig. 12. It is interesting to note that a single factor was sufficient to normalize even element to odd element results. A plot of results at 30 kev is similar to the one for 65-kev neutrons.

Errors

The absolute (*standard deviation*) error in the value of the cross section standard has been indicated to be about 6%. For the measurement of the cross section of other samples relative to the indium standard, at the threshold energies, 30 and 65 kev, other sources of error must be considered:

(1) The error in the determination of the net area under the time spectrum peak is estimated to be about 5% except where noted.

(2) The uncertainties in calculating the R.S.P. (resonance self-protection) correction for the sample relative to indium, as discussed in Appendix III, are estimated to be of order 2%.

(3) The uncertainties in the tank efficiency for a sample as compared to indium are determined by two considerations. The difference in the probabilities of escape of all of the gamma-ray energy of the sample relative to indium appears to be a small effect ($\lesssim 3\%$).[23] However, for samples such as iron where there is a preponderance of ground-state transitions, the total escape probability becomes appreciable (see Fig. 5). The principal uncertainty in the tank efficiency, however, is the uncertainty in the fraction of pulses lying above the bias level, which is estimated to be of order 5% for typical samples compared to indium. The total efficiency error is assigned to be 5%.

(4) The uncertainty in the average path-length correction as discussed in Appendix II is taken as 2%.

The uncertainties in sample weight and geometry are negligible.

The above errors are taken as uncorrelated and added (root-mean-square) to give an estimated typical standard deviation of $\pm 10\%$.

B. Measurement of Radiative Capture Cross Sections as a Function of Energy

All of the measurements of capture cross sections as a function of energy were made relative to the *shape* of the capture cross section of indium. Considerable effort was therefore expended in determining the shape of the indium capture cross section relative to the shape of the total absorption cross section of U^{235} above 100 kev, and relative to the shape of the $B^{10}(n,\alpha_1\gamma)Li^7$ cross section below 140 kev.

For the purpose of comparing the indium cross section to the $B^{10}(n,\alpha_1\gamma)Li^7$ cross section in the region from 7 to 140 kev thick targets of Li^7 and 40-kev thick tritium targets were used. The Li^7 targets provided neutrons in the range from 7 to 70 kev, and the tritium targets

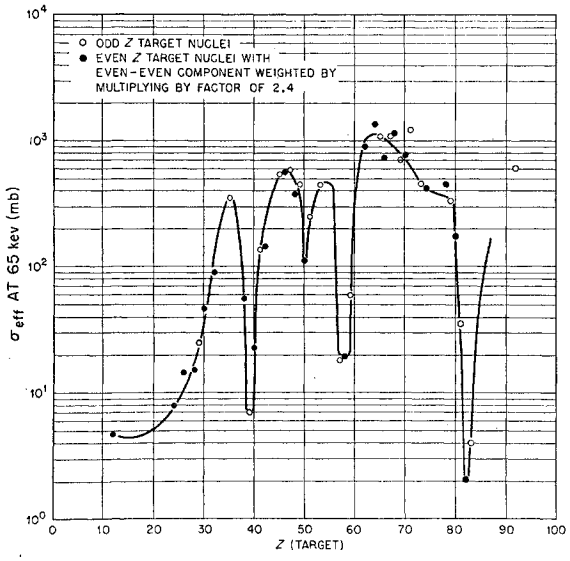

FIG. 12. Average capture cross sections near 65 kev as a function of Z. An empirical factor of 2.4 was determined for correlating cross sections of even-even vs odd-A target nuclei. This factor appears to be approximately independent of A. Other regularities seen are the effects of neutron shells at 50, 82, and 126, as well as the proton shell at $Z=50$.

provided neutrons from 20 kev through 170 kev. The neutron producing target was placed 1.2 meters in front of the sample position and the lithium-loaded paraffin collimator was used to physically collimate the neutrons as indicated in Fig. 1(b). The neutron energies were determined from their flight times. Backgrounds were determined by substituting a lead or carbon disk neutron scatterer for the sample in order to find the shape of the background as a function of neutron flight time, and the magnitude of the background was determined by inspecting flight times when no primary neutrons were arriving at the sample. Successive measurements were made of: (1) the number of indium capture events in the scintillator tank (within the γ-ray single-channel window of 3.7–10 Mev) as a function of neutron flight time, and (2) the shape of the associated neutron flux. For this flux shape measurement a B^{10} slab was viewed by a NaI(Tl) crystal on a photomultiplier, and the number of 478-kev gamma rays as a function of flight time was recorded in the 256-channel analyzer. This detection system has been previously described by Good, Neiler, and Gibbons.[24] The absolute value of the indium capture cross section was normalized to its values for threshold neutrons (30 and 65 kev) whose measurements were described in an earlier section.

The shape of the $B^{10}(n,\alpha_1\gamma)Li^7$ cross section as a function of energy was obtained in the following manner. The $B^{10}(n,\alpha_0)Li^7$ cross section was calculated from reciprocity using the $Li^7(\alpha,n)B^{10}$ cross-section measurements.[33] This was subtracted from the cross section for producing α particles which was measured

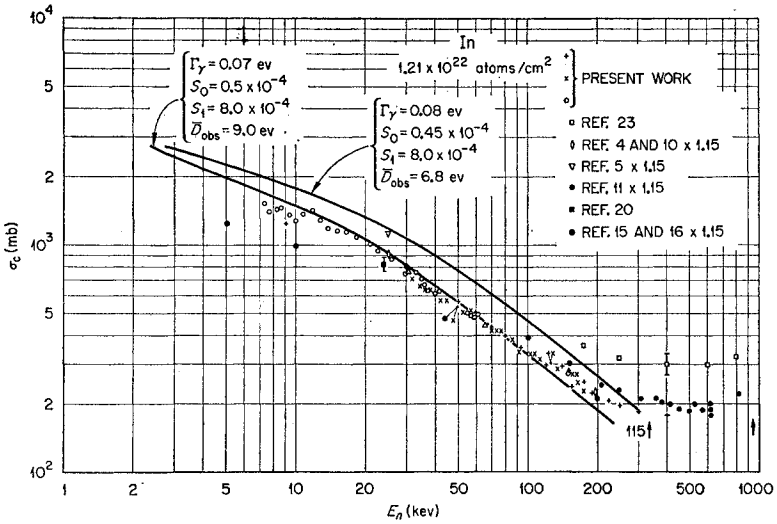

FIG. 13. Capture cross section of indium as a function of energy. Results of various experiments are given as separate symbols for comparison. Energies corresponding to threshold for inelastic scattering are indicated by arrows. The solid curves are theoretical fits to the data, as described in the text.

most recently by Bichsel and Bonner.[34] The result is the shape of the $B^{10}(n,\alpha_1)Li^{7*}$ cross section. Bilpuch *et al.*[15] have investigated carefully the shape of the cross section $B^{10}(n,\alpha)Li^7$, Li^{7*}, from 1 kev to 1 Mev. They find a good fit ($\sim\pm5\%$) to $1/v$ behavior to above 200 kev. Thus based on these results plus corroborative evidence from the graphite sphere measurements given above, we conclude that the *shape* of the $B^{10}(n,\alpha,\gamma)Li^7$ cross section is known to about $\pm5\%$ below 100 kev and perhaps $\pm10\%$ above 100 kev.

For comparing the shape of the capture cross section of indium to that of the absorption cross section of U^{235}, a series of measurements were made with a thin (~3 kev) lithium target and the lithium-loaded paraffin collimator. The neutron flight time over the 1.2-meter flight path was used, in this case, only to separate capture events from background, and to separate the two neutron groups for $E_n<120$ kev. The neutron energy was determined from the proton bombarding energy. The neutron energy range covered in this measurement was 50 to 400 kev. The absorption cross section of U^{235} was constructed from

$$\sigma_a=\sigma_f(1+\alpha). \tag{2}$$

The fission cross section σ_f was taken from the solid line in the Brookhaven compilation.[36] This solid line was constructed utilizing the results of measurements from a number of laboratories.

The straight line, $\alpha=0.190-0.116E_n(\text{Mev})$, given by Diven *et al.*,[37] was used for $E_n>100$ kev. The indium cross section is then given by

$$\sigma_c(\text{In})=K\sigma_a(U^{235})(N_{\text{In}}/N_{\text{U}})(\text{A.P.L.}). \tag{3}$$

$N_{\text{In}}/N_{\text{U}}$ is the ratio of capture counts from indium per microcoulomb of protons (corrected for analyzer dead time) on the lithium target, to the number of absorption counts from the U^{235} sample, per corrected microcoulomb of protons. K is a normalizing constant which was chosen to match the cross section of indium vs U^{235} absorption to that of the indium capture versus the $B^{10}(n,\alpha_1\gamma)Li^7$ cross section, described above, in the range from 100 to 140 kev. (A.P.L.) is the ratio of the average path length, or scattering corrections, and is described in the Appendix II. Both of the resonance self-protection corrections are negligible for neutron energies above 50 kev.

It was possible, as a check on the consistency of the experiment, to calculate the *absolute* indium cross section from the U^{235} absorption cross section using Eq. (1). When this was done, the resulting indium cross section was 7% higher, which is well within the errors. The principle uncertainty in this absolute determination is the value of f_U, the spectrum fraction associated with U^{235} absorption gamma rays. The measurement of the U^{235} absorption gamma spectrum is made difficult by the U^{235} sample background. Implicit also in this analysis is the assumption of equal total efficiencies for the detection of capture and fission events in the U^{235} sample. Since the total efficiency of the tank is high, and the multiplicities of both fission and capture gamma rays are large, this is considered to be a fair assumption, and at worst the assumption should be independent of neutron energy. Because of this uncertainty in f_U and counting rate difficulties due to the natural radioactivity, the normalization to the spherical shell transmission values, discussed in the previous section, was adopted as standard rather than the uranium absorption cross section. The indium cross section resulting from these measurements together with other measurements is shown in Fig. 13.

The capture cross sections of other materials were measured with thick lithium and tritium targets using

[36] *Neutron Cross Sections*, compiled by D. J. Hughes and R. Schwartz, Brookhaven National Laboratory Report BNL-325 (Superintendent of Documents, U. S. Government Printing Office, Washington, D. C., 1958), 2nd ed.

[37] B. C. Diven, J. Terrel, and A. Hemmendinger, Phys. Rev. **109**, 144 (1958).

the lithium-loaded paraffin collimator as described above in connection with the measurement of the indium capture cross section relative to the $B^{10}(n,\alpha_1\gamma)Li^7$ cross section. The single-channel analyzer was set to include gamma rays with pulse heights from 3.7 to 10 Mev to obtain a good ratio of gamma-ray counts to background. The absolute value of this bias level was not important, as the absolute values of the cross sections as a function of energy were normalized to the 30- and 65-kev threshold results described in the previous section.

The neutron flux as a function of energy was determined by taking the indium cross section as a known secondary standard. The cross section of element X for neutrons with energy such that they fall in the ith flight time channel of the multichannel analyzer, is given by

$$\sigma_{xi}=\frac{(A_{xi}-a_i/k_{ax})}{A_{\mathrm{In}i}-a_i/k_{a\mathrm{In}}}k_b\sigma_{\mathrm{In}}. \tag{4}$$

A_{xi} and $A_{\mathrm{In}i}$ are the number of counts in the ith channel from sample X and from the indium standard respectively. a_i/k_{ax} and $a_i/k_{a\mathrm{In}}$ are the normalized backgrounds. k_B is a normalizing constant calculated from the threshold cross sections. An indium flux-shape determination was made about every fourth sample run.

The initial cross sections thus determined were corrected for average path length and resonance self-absorption as described in the appendices.

Cross sections of 22 elements were measured in this manner. The results are shown schematically in a three dimensional plot, Fig. 14. In many cases, particularly the even rare earths, there are no other data with which these data may be compared. For multi-isotope elements there exist few comparisons since the majority of other measurements in this energy range have been made by activation techniques. However, there are comparisons with activation experiments available for many of the odd-A elements, some isolated comparisons with spherical shell transmission results, and in many cases there exists a small range of overlap at low energies with preliminary capture tank results of Block *et al.*[38]

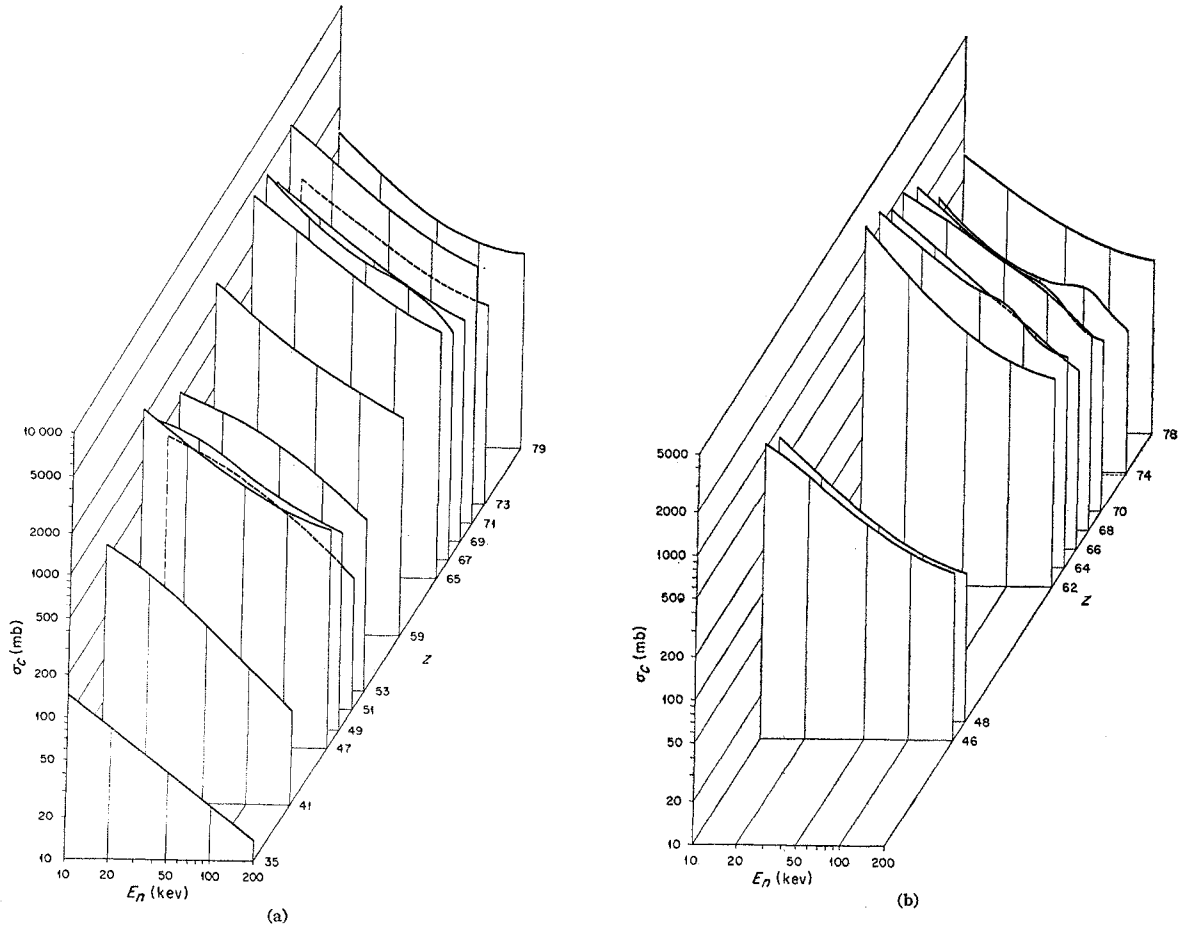

FIG. 14. Capture cross sections of various elements as a function of neutron energy. The results are presented in this fashion for conciseness only. Cross sections of odd-Z elements are shown on (a) and of even-Z elements on (b).

[38] R. C. Block, Bull. Am. Phys. Soc. 4, 474 (1959).

The cross-section results reported here near 200 kev are generally about 30% lower in value than those reported by Diven *et al.*[23] One reason for a part of this difference may be the fact that the two sets of data are not normalized to the same standard; the data reported here are normalized to results of spherical shell transmission measurements at 24 kev while the work of Diven is related to the absorption cross section of U^{235} at 400 kev. The disagreement is large and is not yet understood.

Preliminary results obtained by Block[38] on capture cross sections up to 10 kev for Ag, In, Ta, W, Pt, and Au are in excellent agreement (both shape and magnitude) with the results reported here.

Comparison with the results of Johnsrud *et al.*[11] indicates that the cross sections reported here are either equal to or lower than their results. Elements compared are Br, In, I, Pr, and Au. Relatively good agreement occurs for In, Pr, and Au but our results for Br and I are more than 25% lower than theirs. It should be mentioned that effects of multiple scattering (average neutron path length) could be important in their experiment but apparently were not considered in any detail.

Comparison with activation results using photoneutron sources[4,5,10] shows agreement ranging from excellent (e.g., In, I) to very poor (e.g., Sb, Au). Where disagreement occurs the activation results are usually higher than those reported in this paper.

Although a weighted average of five of the spherical shell absorption cross sections[20] was used for normalization, it is useful to compare the results element by element, especially with shell results not used in determining the normalization factor. The agreement between the results reported here and the shell results is good. In only one case, Cd, was the disagreement greater than about 10%, still well within the experimental errors quoted. No comparison has been made with the results of Belanova[21] since there appear to be several serious difficulties[20] associated with those results as to the cross-section value, experimental errors, and effective neutron energy.

The activation studies of iodine and gold by Bame and Cubitt,[8] normalized to U^{235} fission cross section, are in rather good agreement with the capture tank work of Diven *et al.*, but lie about 25% higher than the results reported here.

Gabbard, Davis, and Bonner,[9] who measured the activation cross section of iodine with a LiI(Eu) crystal with neutron flux determination by a modified long counter, are in good agreement with the results reported here for energies up to about 100 kev. At higher energies their data show a less rapidly decreasing cross section, resulting in a 25% difference at 200 kev. Activation results by Miskel *et al.*[12] on tantalum and gold are in disagreement with the results reported here, both in regard to cross-section shape and value, particularly in the case of gold. Recent gold-activation measurements by Cox,[39] normalized to the U^{235} fission cross section, are in good agreement with the results of Miskel *et al.*[12] The cause of this disagreement is not known but is under continuing study.

It is possible to compare our results in detail with the relative cross sections of Bilpuch *et al.*,[15] and Weston *et al.*[16] in three cases, In, I, and Au. In the case of indium, it should be noted that an incorrect normalization was used in their experiment. Excellent agreement is seen for the case of iodine. The magnitude of the crosssection results for gold are in disagreement but only because of the different normalization used.

In summary, although considerable differences still exist between various results the spread in results is steadily decreasing as more and more of the subtle but important experimental effects such as those considered in Appendixes II and III are found. The spread in results reflects somewhat the difficulty encountered in making accurate measurements in the kev range. It is disturbing, however, that results on such frequently studied nuclei as gold are still in such poor agreement. Indeed, in the case of gold, results appear to be evolving into two bands over the energy range from 10 to 200 kev.

Errors

The errors in the cross sections as a function of energy are obviously dependent on the element, and on the neutron energy. The errors are minimum at the points of normalization, namely 30 and 65 kev, and, as was discussed before, the standard deviation errors at these energies are estimated to be about 10%. At energies below 15 kev, the signal to background ratio from the thick Li targets used was poorer, and the error rises to perhaps 15%. Between 100 and 140 kev the shapes of the $B^{10}(n,\alpha_1\gamma)Li^7$ and U^{235} absorption cross sections are least well known and the errors have, perhaps, a maximum. The agreement of the thick tritium target measurements with the thin lithium target results at 167 kev where the U^{235} absorption cross section is relatively well known, indicates that the errors are small at high energies.

A qualitative estimate of the error as a function of energy, *including the 10% normalization to indium*, is shown in Fig. 15.

Analysis and Discussion

The experimental cross-section results show general similarities in shape from element to element. For instance, the rough average shape of the cross section is

$$\sigma(E)=K_1E_n^{-K_2}. \tag{5}$$

It is apparent, however, that significant changes do occur from element to element. The onset of inelastic scattering by rotational levels is quite marked for some cases (Fig. 16), but it is not observed for levels in other

[39] S. A. Cox (private communication).

nuclei such as the 75-kev level in Au^{197} (see Fig. 17). For energies below excited states and less than about 100 kev, where d-wave neutrons are usually not important, the capture cross section should be susceptible to decomposition into simple s- and p-wave partial cross sections. The cross section for neutrons of angular momentum l, captured by levels of total angular momentum J, can be written as[40]

$$\sigma_{Jl}=\frac{2\pi^2}{k^2}g_J\sum_j\frac{\langle\Gamma_J(n,l,j)\rangle\langle\Gamma_J(\gamma)\rangle}{\langle D_J\rangle\langle\Gamma_J\rangle}F(\alpha_{lJ}), \qquad (6)$$

where

$$F(\alpha_{lJ})=\left\langle\frac{\Gamma_J(n,l,j)\Gamma_J(\gamma)}{\Gamma_J}\right\rangle\Big/\frac{\langle\Gamma_J(n,l,j)\rangle\langle\Gamma_J(\gamma)\rangle}{\langle\Gamma_J\rangle},$$

and

$$\alpha_{lJ}=\frac{\langle\Gamma_J(\gamma)\rangle}{\langle\epsilon^l{}_{lJ}\Gamma_J(n,l,j)\rangle};$$

$\epsilon^l{}_{lJ}$ will be defined below, and the sum over j is a sum over channel spins for a given J and l. The rest of the symbols have their usual meaning. For the case of s-wave neutrons, where $J=j$, since $l=0$, Eq. (6) reduces to

$$\langle\sigma_{J0}\rangle=\frac{2\pi^2}{k^2}\langle\Gamma_\gamma\rangle\left\langle\frac{\Gamma_n{}^0}{D}\right\rangle E_n{}^{\frac{1}{2}}\times\sum_J\frac{g_JF(\alpha_{0J})}{\langle\Gamma_n{}^0/D\rangle(D_{\rm obs}/g_J)E_n{}^{\frac{1}{2}}+\langle\Gamma_\gamma\rangle}. \qquad (7)$$

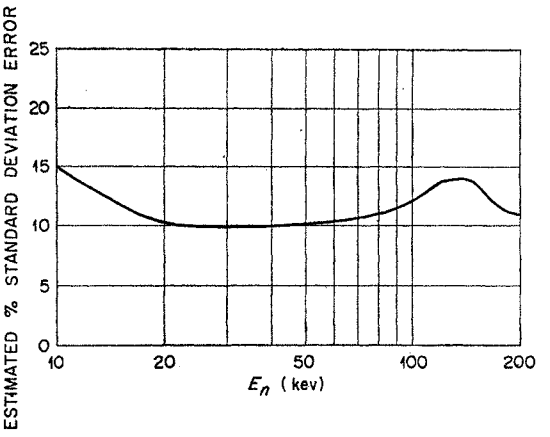

FIG. 15. Estimated total error (S.D.) associated with the cross section results as a function of neutron energy. The error is energy sensitive because of factors such as neutron yield (signal to background) and relative neutron flux calibration as discussed in the text.

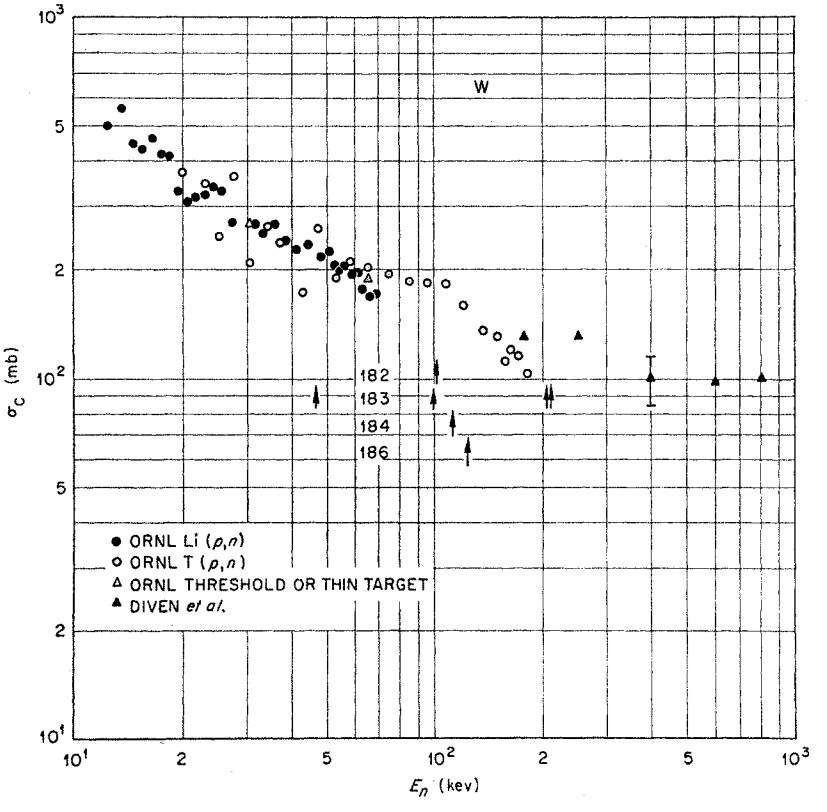

FIG. 16. Capture cross section of tungsten as a function of energy. The downward break in the cross section near 100 kev is a good example of the effect of competition from the onset of inelastic scattering.

[40] A. M. Lane and J. E. Lynn, Proc. Phys. Soc. (London) **A70**, 557 (1957).

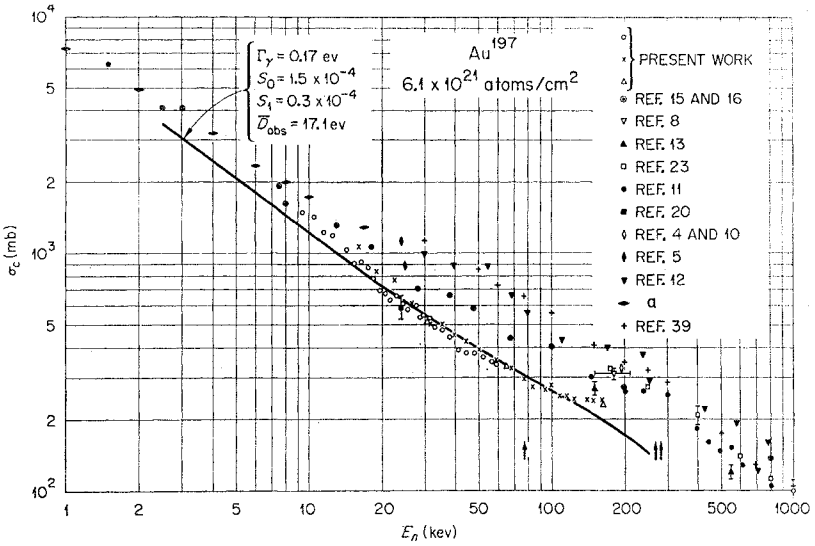

FIG. 17. Capture cross section of gold as a function of energy. Results of various other experimenters are given. [I. A. Isakov, V. P. Popov, and F. L. Shapiro, J. Exptl. Theo. Phys. (U.S.S.R.) 38, 189 (1960).] The solid line corresponds to the calculated cross section using latest estimates from low-energy total cross-section measurements (see reference 45), and a reasonable p-wave strength function.

Equation (7) is subject to the following assumptions:

(1) $\langle\Gamma^0_{nJ}/D_J\rangle$ is independent of J and $\langle\Gamma^0_{nJ}/D_J\rangle\ll 1$.

(2) $$D_J=\frac{2(2I+1)D_{\rm obs}}{2J+1}=\frac{D_{\rm obs}}{g_J}.$$

(3) Γ_γ is independent of J.

(4) Γ_γ is independent of energy. This assumption should be valid as long as the range of neutron energy is small compared to the neutron binding energy. D_J is also independent of neutron energy for the same reason.

(5) $\Gamma=\Gamma_n+\Gamma_\gamma$. This simply states that inelastic scattering is forbidden or ignored in our range of interest. It has previously been noted that there are elements where this assumption breaks down at the higher energies. For p-wave neutrons, Eq. (6) becomes

$$\sigma_{l=1}=\frac{2\pi^2\langle\Gamma_\gamma\rangle}{k^2}\left(\frac{E_n{}^{\frac{1}{2}}x^2}{1+x^2}\right)\sum_J\frac{\epsilon^1{}_{JI}g_JS_1F(\alpha_iJ)}{\langle\Gamma_J\rangle},\qquad(8)$$

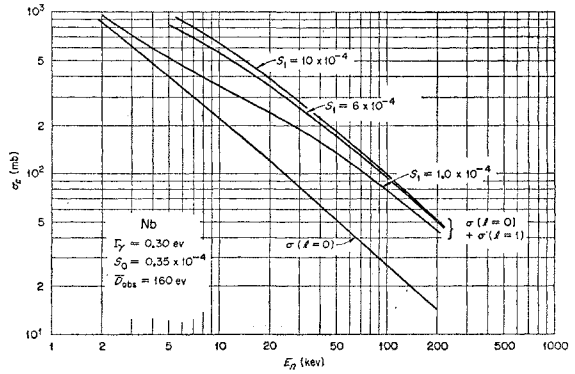

FIG. 18. Calculated capture cross section for niobium for various assumed values of the p-wave strength function.

where

$$x=kr=k(1.35A^{\frac{1}{3}}\times 10^{-13}),$$

$$\langle\Gamma_J\rangle=\langle\Gamma_{nJ}\rangle+\langle\Gamma_\gamma\rangle=\sum_j\langle\Gamma_{nJj}\rangle+\langle\Gamma_\gamma\rangle$$
$$=\epsilon^1{}_{JI}\langle\Gamma_{nJj}\rangle+\langle\Gamma_\gamma\rangle,\qquad(9)$$

where it is assumed that $\langle\Gamma_{nJj}\rangle$ is independent of j,

$$g_J=\frac{(2J+1)}{2(2I+1)}(\text{scalar quantities}),$$

and where

$\epsilon^l{}_{JI}=2$ for $|J-l|\leqq I\pm\frac{1}{2}\leqq J+l$

$=1$ for $|J-l|\leqq$ either $(I+\frac{1}{2})$ or $(I-\frac{1}{2})$ but not both $\leqq J+l$

$=0$ otherwise.

It should be noted that $\sum_J\epsilon^l{}_{JI}g_J=(2l+1)$. We now define the p-wave strength function to be

$$S_1=\langle\Gamma^1{}_{nJj}/D_J\rangle,\qquad(10)$$

which is assumed to be independent of j.

The following additional assumptions are implicit in these formulas:

1. $D^\pi{}_J$ is independent of parity π for a given J. This assumption is more likely to be true for odd-Z elements,[41,42] which are the only elements for which theoretical fits were attempted.

2. The average neutron width per channel-spin projection is independent of the channel spin. This implies that the neutron strength function for states of a given J is proportional to the number of ways of forming states of angular momentum J from an orbital

[41] H. W. Newson and M. M. Duncan, Phys. Rev. Letters 3, 45 (1959).

[42] H. W. Newson, E. G. Bilpuch, and L. W. Weston, Bull. Am. Phys. Soc. 4, 475 (1959).

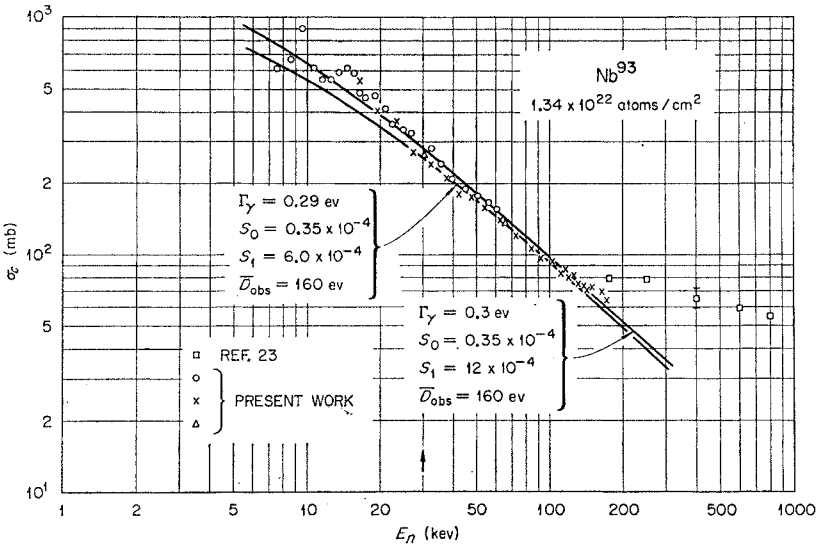

FIG. 19. Capture cross section of niobium as a function of energy. The solid curves were calculated using average nuclear parameters derived from low-energy total cross-section measurements (see reference 46), and two different values for S_1. This indicates that, for large values of S_1, more data are needed in the energy range from 1 to 10 kev.

angular momentum l and all possible contributing channel spins. This assumption is implied by the factor $\epsilon^l{}_{IJ}$.

3. It has been assumed that Γ_γ is independent of l, i.e., of parity.

4. R, the channel radius as reflected in $x=kR$, has been taken to be $R=1.35\times10^{-13}A^{\frac{1}{3}}$ cm, and independent of J and l. The general shape of the cross section for different values of the p-wave strength functions S_1 is given in Fig. 18. The maximum in the p-wave contribution shifts to higher energies for lower p-wave strength functions. For the usual range of values for strength functions, etc., the p-wave maximum appears in the range 10–100 kev. Thus, s- and p-wave average effects on capture cross sections are best observed in this region.

The procedure for the fitting of experimental data was as follows: (a) using s-wave parameters, the $l=0$ cross-section contribution was calculated, (b) to this was added a cross section for $l=1$ neutrons obtained by "first guess" of the p-wave strength function. In many cases, such as gold (Fig. 17), niobium (Fig. 19), antimony (Fig. 20), iodine (Fig. 21), tantalum (Fig. 22), praseodymium (Fig. 23), and silver (Fig. 24), only minor adjustments, if any, in s-wave parameters were needed to obtain good fits with parameter values within limit of error. However, for others, and especially the rare earths (see, for example, Fig. 25), fits were obtainable only by assuming that either (1) average level spacing or radiative widths were wrong by up to a factor of four, or (2) that level spacing and radiative widths were simultaneously wrong by up to a factor of two. Once satisfactory fits were determined and a value of S_1 was derived, the cross section was recalculated using the "chopper parameters" and the value of S_1. Curve fits have been made on thirteen of the twenty-one elements studied as a function of energy.

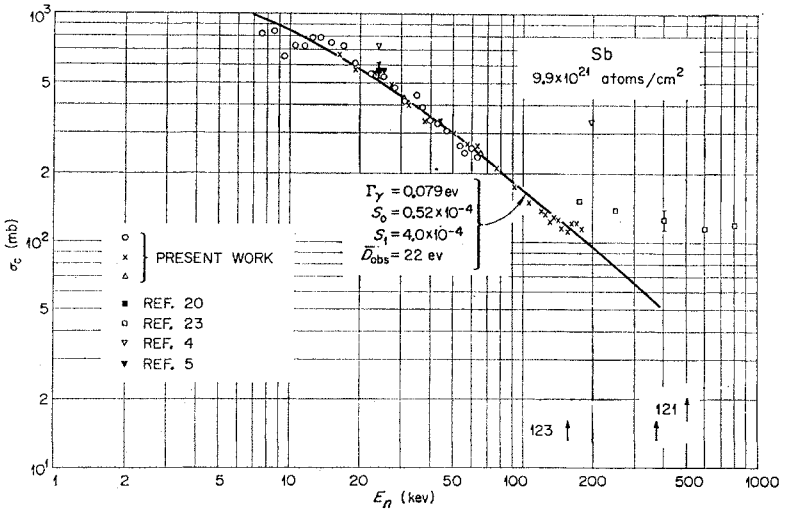

FIG. 20. Capture cross section of antimony as a function of energy.

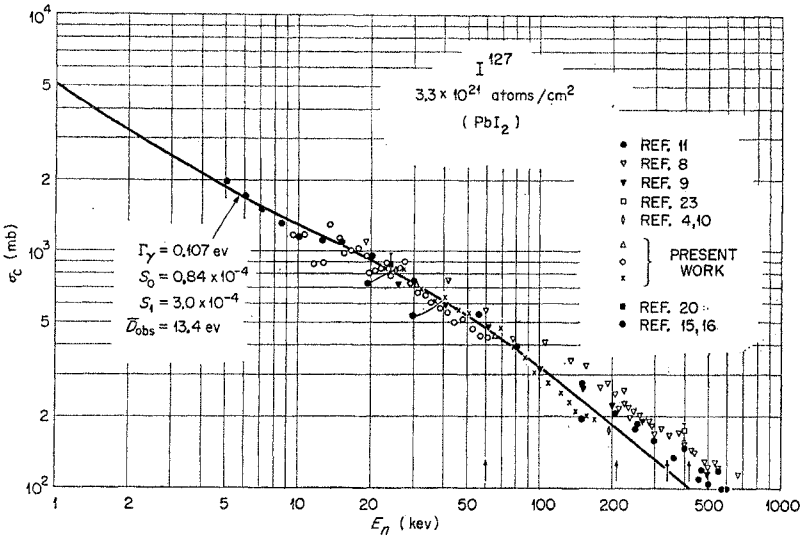

FIG. 21. Capture cross section of iodine as a function of energy. Results of other experiments are given for comparison. The solid curve was calculated using recent results of low-energy total cross section measurements (see reference 47) and a p-wave strength function of 3.0×10^{-4}.

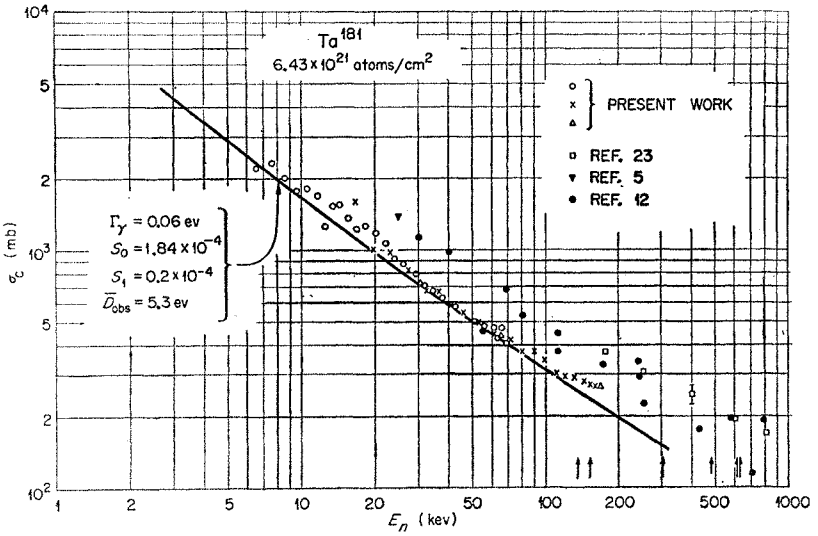

FIG. 22. Capture cross section of tantalum as a function of energy. The results of other experiments are given for comparison. The lower solid curve was calculated using results (see Table III) of low-energy total cross section measurements and a p-wave strength function of 0.2×10^{-4}.

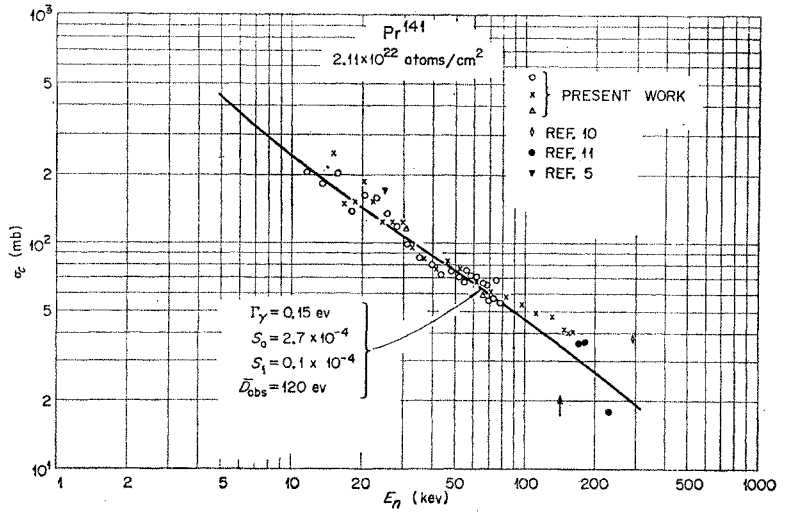

FIG. 23. Capture cross section of praseodymium as a function of energy. Results of other experiments are given for comparison. The solid curve was calculated using results of low-energy total cross section measurements, with a p-wave strength function (for best fit) of 0.1×10^{-4}.

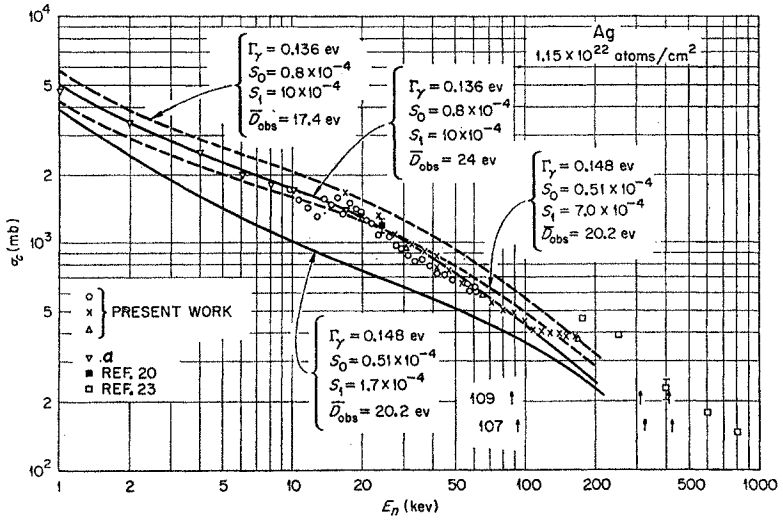

FIG. 24. Capture cross section of silver as a function of energy. The upper dotted curve was calculated using recent low-energy total cross section results (see footnote a, Table III) and a p-wave strength function of 1.0×10^{-3}. The upper solid curve was computed using low-energy parameters modified to take into account the occurrence of p-wave resonances in the ev range. The lower solid curve was calculated using another recent set of low-energy measurements (see reference 45) in which the p-wave strength function was also given. [I. A. Isakov, V. P. Popov, and F. L. Shapiro, J. Exptl. Theoret. Phys. (U.S.S.R.) **38**, 189 (1960).] The lower dotted curve was computed by increasing the value of S_1 from 1.7×10^{-4} (given in reference 45) to 7×10^{-4} in an attempt to obtain a more reasonable fit to the data.

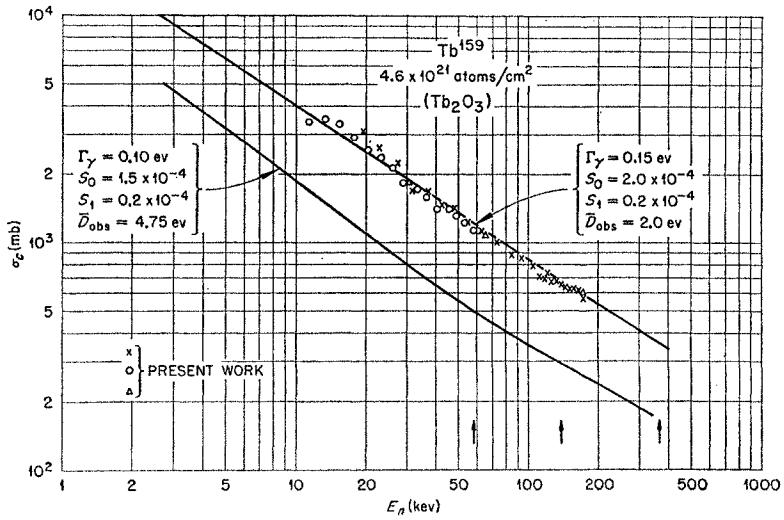

FIG. 25. Capture cross section of terbium as a function of energy. The lower curve was calculated using results of low-energy cross section measurements for s-wave parameters and a reasonable p-wave strength function. The upper curve is a fit obtained by changing s-wave parameters. The change required was far outside error limits quoted for the low-energy total cross section results.

Attempts have not been made to fit the results in cases of even elements with several isotopes. Of the thirteen elements fitted a representative group is given in Figs. 13, 16, 17, 19–25.

There is some basis for the assumption of rather large errors associated with some estimates of level spacings and radiative widths as determined from low-energy total cross-section measurements. It can be seen in cases such as indium (Fig. 13), and silver (Fig. 24), that simple counting of all resonances led to too small a value for s-wave level spacing, due to the enhanced number of observable p-wave resonances in the ev range for $A\sim100$. Recently direct observation of this effect has been reported.[43–45] Likewise, for $A\sim160$, the average spacing might tend to be overestimated due to pileup of resonances caused by the s-wave giant resonance maximum. Radiative widths have recently been found to sometimes vary by a significant factor from resonance to resonance even for a nucleus as heavy as gold.[46] Thus, the radiative width of a given resonance may be significantly different from the true average even for heavy elements.

It is perhaps noteworthy and certainly encouraging that in cases where the greatest amount of recent attention has been placed on low-energy resonance parameters and spacings one finds rather good agreement between low-energy parameters and the average capture cross section reported here, both in detailed shape and in magnitude.

The reader is reminded that the fits described here are made under several simplifying assumptions. Thus,

[43] A. Saplakaglu, L. M. Bollinger, and R. E. Coté, Phys. Rev. **109**, 1258 (1958).

[44] J. L. Rosen, S. Desjardins, W. W. Havens, and J. Rainwater, Bull. Am. Phys. Soc. **4**, 473 (1959).

[45] J. S. Desjardins, J. L. Rosen, W. W. Havens, Jr., and J. Rainwater, Phys. Rev. **120**, 2214 (1960).

[46] J. S. Desjardins, J. L. Rosen, James Rainwater, and W. W. Havens, Bull. Am. Phys. Soc. **5**, 32 (1960).

the departure of the cross section from the calculated curve at higher energies is not at all surprising. The onset of inelastic scattering causes a decrease in the cross section (e.g., Fig. 16) while effects due to d-wave neutrons and possible changes in average spacings and gamma-ray width with excitation energy can cause a flattening in the cross section (e.g., Fig. 13). It should also be noted in the rare earth region (where the flattening seen in the higher energy cross section is fit by adjusting the p-wave strength function) that the non-s-wave contribution may be due to d-wave, rather than p-wave neutrons since the d-wave strength function has a peak somewhere in this region.

The curve fits reported here are not unique, in that the cross section is dependent upon the ratio $\langle\Gamma_\gamma/D\rangle$ and not the two parameters separately. *However, we have separately considered* $\langle\Gamma_\gamma\rangle$ *and* $\langle D\rangle$ *since they are independently measured quantities.* None of the parameters are considered really "free" except S_1 since their approximate value is more or less dictated by low-energy total cross-section results. The energy-sensitive effect of changing some of the parameters is given in several of the figures.

Values for parameters used and results of the curve fitting are given in the individual figures and are summarized in Table III. In cases, such as silver and antimony, where odd Z elements consist of two isotopes, low-energy cross-section results for the individual isotopes were averaged by abundance weighting to form an effectively monoisotopic element. The "first choice" parameters with the exception of S_1 (p-wave strength function) were those taken from other low-energy measurements.

The p-wave strength functions (as defined earlier) derived from the curve fits and given in Table III show the obvious presence of a broad maximum near $A=100$. This is the $2p$ giant resonance predicted by the optical model. The apparent width of the peak as indicated by our results suggests complexity, in agreement with results of relative cross-section measurements[15] where it was suggested[16] that the presence of spin-orbit forces produces a $p_{\frac{1}{2}}-p_{\frac{3}{2}}$ splitting of the giant resonance. However, as discussed earlier, there appears to be a serious systematic disagreement between these workers and ourselves in the cross-section results, particularly at lower energies. This disagreement in experimental results is the cause of the difference in the derived value of S_1.

The importance of p-wave effects for energies as low as a few kev is obvious. It is much more difficult to experimentally determine at what neutron energy d-wave contributions become important. The attempts to fit the data using optical-model parameters and results from low-energy total cross sections indicate that the shape of average capture cross section has a much higher sensitivity to the value of the p-wave strength function than is found in corresponding total cross-section shapes. It is apparent, however, that the energy region most sensitive to *large* values of S_1 lies between 1 and 10 kev where experimental techniques are especially difficult.

It is interesting to note that competition from low-energy neutron inelastic scattering can be observed from the capture results. The drop (due to inelastic scattering), such as is observed in Yb at 80 kev (Fig. 26)

TABLE III. Summary of curve-fitting results of cross sections as a function of neutron energy. The left portion of the table gives "first choice" parameters obtained from low-energy total cross section results. The right portion of the table gives "best fit" values for the parameters, obtained by curve fitting of the capture cross section. It is clear, from column 11, that the p-wave strength functions show a large peak in the range $A=90$ to 120. Estimated errors are given for S_1. These errors reflect ranges of S_1 outside of which one cannot obtain a reasonable shape fit to the data.

				"First choice" parameters					"Best fit" parameters				
Element	A_{eff}	I	R (10^{-13} cm)	$S_0(10^{-4})$	Γ_γ(ev)	$\bar{D}$(ev)	$\Gamma_\gamma/\bar{D}(10^{-2})$	Reference	$S_0(10^{-4})$	$S_1(10^{-4})$	$\bar{\Gamma}_\gamma$(ev)	$\bar{D}$(ev)	$\bar{\Gamma}_\gamma/\bar{D}(10^{-2})$
Br	80	3/2	5.8	1.4	0.39	67	0.58	a	1.4	0.05±0.05	0.70	40	1.8
Nb	93	9/2	6.2	0.35	0.3	160	0.19	b, c	0.35	12±5	0.3	160	0.19
Ag	108	1/2	6.2	0.51	0.148	20.2	0.73	a, d	0.8	10±3	0.136	24	0.57
In	115	9/2	6.5	0.45	0.08	6.8	1.2	a	0.5	[8±2	0.07	9.0	0.78
Sb	122	5/2	6.7	0.52	0.079	22	0.36	a	0.52	4.0±1.0	0.079	22	0.36
I	127	5/2	6.8	0.84	0.107	13.4	0.80	e	0.84	3.0±1.5	0.107	13.4	0.80
Pr	141	5/2	7.1	2.7	0.15	120	0.13	a	2.7	0.1±0.1	0.15	120	0.13
Tb	159	3/2	7.3	1.5	0.10	4.75	2.1	a	2.0	0.2±0.2	0.15	2.0	7.5
Ho	165	7/2	7.4	2.3	0.07	6.3	1.1	a	3.0	0.4±0.4	0.15	3.0	5.0
Tm	169	1/2	7.5	1.6	0.07	7.0	1.0	a, f	1.8	0.1±0.01	0.12	3.5	3.4
Lu	175	7/2	7.6	1.8	0.06	3.2	1.9	a	3.0	0.1±0.01	0.12	1.5	8.0
Ta	181	7/2	7.7	1.84	0.06	5.3	1.1	d, g, h	2.0	0.2±0.2	0.065	4.3	1.5
Au	197	3/2	7.9	1.4	0.17	17.1	1.0	d	1.4	0.3±0.3	0.17	17.1	1.0

[a] *Neutron Cross Sections*, compiled by D. J. Hughes, B. A. Magurno, and M. K. Brussel, Brookhaven National Laboratory Report BNL-325 (Superintendent of Documents, U. S. Government Printing Office, Washington, D. C., 1960), 2nd. ed., Suppl. No. 1.
[b] See reference 43.
[c] See reference 46.
[d] See reference 45.
[e] J. L. Rosen (private communication).
[f] J. A. Harvey (private communication).
[g] F. W. K. Firk, Nuclear Phys. 9, 198 (1958).
[h] J. E. Evans, B. B. Kinsey, J. R. Waters, and G. H. Williams, Nuclear Phys. 9, 205 (1958).

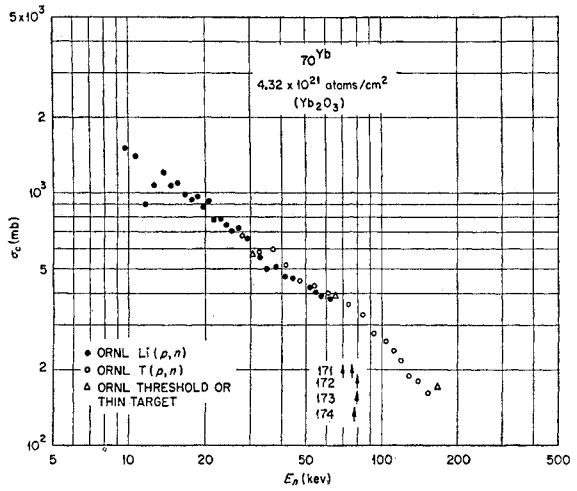

FIG. 26. Capture cross section of ytterbium as a function of energy. The downward break in the curve near 80 kev indicates the onset of inelastic scattering.

and W above 100 kev (Fig. 16), exhibits the competition due to inelastic scattering.

The success in detailed fitting of the experimental results is gratifying and indicates strongly that, for example, average level density and radiative widths do not change significantly in the first 100 kev above the neutron binding energy.

Further investigation of neutron capture in the kev energy range is anticipated, using enriched isotopes and samples of lower atomic weight.

ACKNOWLEDGMENTS

The successful completion of these experiments would not have been possible without the help of many people. N. H. Lazar helped design the capture tank; W. M. Good, C. H. Johnson, R. F. King, J. W. Johnson, and J. P. Judish were instrumental in development and maintenance of the terminal pulsing equipment and ion source. A. F. Nickle and M. C. Taylor were responsible for much of the automatic data processing. T. Emmer gave invaluable help in electronics development and maintenance.

The continued close communication with B. C. Diven, L. Dresner, P. A. Moldauer, H. W. Newson, and H. W. Schmitt contributed significantly to the success of this work.

We would also like to express appreciation for valuable discussions, cooperation, and encouragement to J. L. Fowler and A. M. Weinberg.

APPENDIX I. AVERAGE NEUTRON ENERGY FROM (p,n) REACTIONS NEAR THRESHOLD

It is desired to determine with precision the average energy of the entire neutron yield from the (p,n) reaction near threshold. Define

$$\bar{E}_n=\int E_n dN \Big/ \int dN, \tag{11}$$

where dN is the elemental neutron intensity. For convenience, the integration is performed in the center-of-mass system, with

$$dN=W(\Delta)d\Delta V(\phi)d\phi, \tag{12}$$

where $W(\Delta)d\Delta$ is the total neutron yield for an infinitesimal layer of the target at a depth Δ and thickness $d\Delta$, and $V(\phi)d\phi$ is the center-of-mass angular distribution at each layer. $V(\phi)$ is taken to be isotropic. Now using the standard notation for E_n,[47] Eq. (11) can be reduced to

$$\bar{E}_n=C+D\left(\int_{\Delta_1}^{\Delta_2}\Delta W(\Delta)d\Delta \Big/ \int_{\Delta_1}^{\Delta_2} W(\Delta)d\Delta\right), \tag{13}$$

where

$$C\equiv\frac{M_pM_n}{(M_p+M_t)^2}E_{\text{th}} \quad \text{and} \quad D\equiv\frac{M_pM_n+M_tM_r}{(M_p+M_t)^2}.$$

(Δ_2+E_{th}) is the initial proton energy and $(\Delta_2-\Delta_1)$ is the target thickness for protons. The yield function, $W(\Delta)$, contains the energy dependence of the (p,n) cross section and the proton energy loss as a function of depth in the target.

For the case of $T(p,n)$ the cross section rises[48] as the s-wave penetrability $(\Delta^{\frac{1}{2}})$. The $Li(p,n)$ cross section,[48] on the other hand, is proportional to $\Delta^{\frac{1}{2}}/[\Delta^{\frac{1}{2}}+(90)^{\frac{1}{2}}]^2$.

Using a constant dE_p/dx, the s-wave case [e.g., $T(p,n)$] gives

$$\bar{E}_n=C+\tfrac{2}{5}D\left[\frac{\Delta_2^{\frac{5}{2}}-\Delta_1^{\frac{5}{2}}}{\Delta_2^{\frac{3}{2}}-\Delta_1^{\frac{3}{2}}}\right]. \tag{14}$$

Likewise for the case of $Li^7(p,n)$ we have, assuming a thick target $(\Delta_1=0)$,

$$\bar{E}_n=C+\tfrac{2}{5}D\Delta_2 \times\left[\frac{1-5X/3+15X^2/7-5X^3/2+\cdots}{1-3X/2+9X^2/5-2X^3+\cdots}\right]_{X=(\Delta_2/90)^{\frac{1}{2}}}. \tag{15}$$

Applying these equations to $T(p,n)He^3$ with $\Delta E_p=2.4$ kev gives $\bar{E}_n=65$ kev and for $Li^7(p,n)Be^7$ with $\Delta E_P\simeq2$ kev, $\bar{E}_n=30.5$ kev.

APPENDIX II. DETERMINATION OF AVERAGE NEUTRON PATH LENGTH[49]

In the class of neutron cross-section measurements involving 4π detection of reaction products, such as is encountered in the radiative capture tank technique, the effects of single and multiple neutron scattering can be large, *even for thin, high-transmission samples.* An analytical expression for the average path length

[47] See, for example, J. B. Marion and J. L. Fowler, *Fast Neutron Physics* (Interscience Publishers, Inc., New York, 1960), Vol. I, p. 133 ff.

[48] R. L. Macklin and J. H. Gibbons, Phys. Rev. **109**, 105 (1958).

[49] The contents of this correction were developed by H. W. Schmitt, Oak Ridge National Laboratory Report ORNL-2883 (1960), (unpublished).

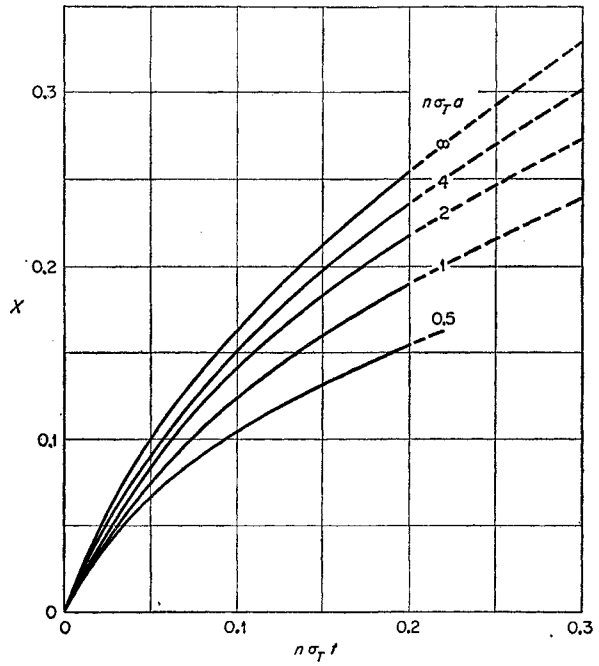

FIG. 27. The average path length correction factor X, defined as $(\sigma_s/\sigma_T)[1-\langle e^{-n\sigma_T R}\rangle]$, as a function of $n\sigma_T t$.

has been derived for the case of plane parallel neutrons axially incident upon a thin disk of material whose scattering and capture cross sections are considered to be constant over several neutron collisions. Later Monte Carlo calculations for a finite neutron beam diameter produced essentially identical results. A summary of the derivation is as follows: Axial neutrons are considered incident upon the sample disk in which only elastic scattering and capture can occur. Then the *total* number of captures per incident neutron f_c is

$$f_c=(1-e^{-n\sigma_T t})\frac{\sigma_c}{\sigma_T}+(1-e^{-n\sigma_T t})\frac{\sigma_s}{\sigma_T}\left[(1-\langle e^{-n\sigma_T R_1}\rangle)\frac{\sigma_c}{\sigma_T}+\cdots\right], \quad (16)$$

where R_1 is the geometric path length in the disk for a neutron which has been scattered once. For relatively thin disks ($\sim$0.1 mean free path) it has been shown that[49]

$$\langle e^{-n\sigma_T R_1}\rangle=\langle e^{-n\sigma_T R_2}\rangle=\cdots=\langle e^{-n\sigma_T R_i}\rangle. \quad (17)$$

Then defining $X=(\sigma_s/\sigma_T)(1-\langle e^{-n\sigma_T R}\rangle)$, we have

$$f_c=(1-e^{-n\sigma_T t})\frac{\sigma_c}{\sigma_T}[1+X+X^2+\cdots]=(1-\langle e^{-n\sigma_T t}\rangle)\frac{\sigma_c}{\sigma_T}\left(\frac{1}{1-X}\right). \quad (18)$$

The quantity to be determined then is $\langle e^{-n\sigma_T R}\rangle$. This has been determined explicitly for cylindrical geometry.[49] The results for a disk of radius a and thickness t are

$$\langle e^{-n\sigma_T R}\rangle=\frac{1+e^{-n\sigma_T t}}{2(1-e^{-n\sigma_T t})}\left\{1-e^{-n\sigma_T t}\left[1-\frac{t}{2a}(n\sigma_T t)\right]-e^{-n\sigma_T a}+\exp[-n\sigma_T(a^2+t^2)^{\frac{1}{2}}]-X_1+X_2\right\}\cdots, \quad (19)$$

where

$$X_1=\frac{(n\sigma_T t)^2}{2}[-\ln(n\sigma_T t)+(\tfrac{1}{2}-\gamma)]\sum_{n=1}^{\infty}\frac{(-1)^{n-1}(n\sigma_T t)^{n+2}}{n!n(n+2)},$$

where γ is Euler's number, 0.5772;

$$X_2=\int_{Z=0}^{t} n\sigma_T Z\{-E_i[-n\sigma_T(Z^2+a^2)^{\frac{1}{2}}]\}n\sigma_T dZ. \quad (20)$$

Under usual conditions the value of X_2 is much less than X_1. The results given above are valid to better than 1% for $n\sigma_T t\lesssim 0.2$, $a\gtrsim 2t$. The parameter X defined in the text following Eq. (17) as a function of $(n\sigma_T t)$ is given in Fig. 27 for the case $\sigma_s/\sigma_T\approx 1.0$.

APPENDIX III. RESONANCE SELF-PROTECTION CORRECTION

Corrections for resonance self-protection must be considered in all average capture cross-section experiments. The magnitude of the correction is a function of many variables such as sample thickness, ratio of resonance to off resonance total cross section, ratio of capture to scattering widths, neutron width distributions, strength functions, angular momenta, and energy. It has been considered in detail by Dresner[50] and

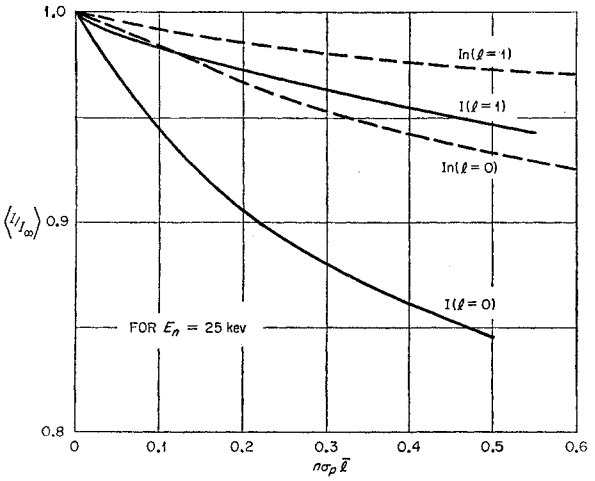

FIG. 28. The resonance self-protection correction factor $\langle I/I_\infty\rangle$ as a function of sample thickness for thin samples of indium and iodine at 25 kev.

[50] L. Dresner, Oak Ridge National Laboratory Report ORNL-2659 (1959), (unpublished).

applied to spherical shell absorption measurements at 24 kev by Schmitt and Cook.[20]

For the purpose of illustration the self-protection correction factors $\langle I/I_\infty \rangle$ for indium and iodine at 25 kev are given as a function of sample thickness (Fig. 28). *The factor $\langle I/I_\infty \rangle$ represents effectively the ratio of apparent cross section to the true cross section for an infinitely dilute sample.* The factor (R.S.P.) given in Eq. (1) of the text is simply the ratio of $\langle I/I_\infty \rangle$ for the standard to that of the sample. The effects of s-wave and p-wave neutrons are computed separately and then weighted to obtain the over-all sample correction in the following manner.

$$\langle I/I_\infty \rangle = \frac{\sigma_c(l=0)\langle I/I_\infty \rangle_{l=0} + \sigma_c(l=1)\langle I/I_\infty \rangle_{l=1}}{\sigma_c(l=0)+\sigma_c(l=1)}. \quad (21)$$

In the expression given above, $\sigma_c(l=0)$ and $\sigma_c(l=1)$ are, respectively, the s-wave and p-wave partial capture cross sections, whose sum is equal to the total capture cross section in the energy range under consideration. The correction for the indium sample used in the work reported here ($n\sigma_p \bar{l}=0.068$) is given in Fig. 29, showing the dependence of the correction as a function of neutron energy. The reader is referred to the references mentioned above for specific details of the correction.

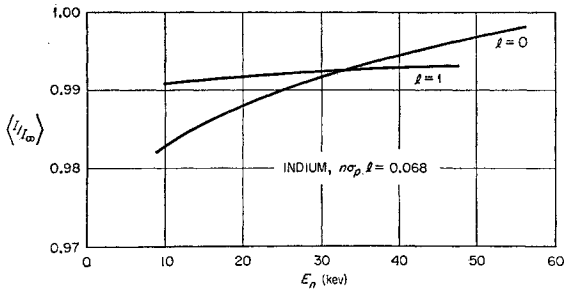

FIG. 29. The resonance self-protection correction factor $\langle I/I_\infty \rangle$ as a function of neutron energy for indium.